Structure-based energetics of protein interfaces guides foot-and-mouth disease virus vaccine design

Abhay Kotecha[1,8], Julian Seago[2,8], Katherine Scott[3], Alison Burman[2], Silvia Loureiro[4], Jingshan Ren[1], Claudine Porta[1,2], Helen M Ginn[1], Terry Jackson[2], Eva Perez-Martin[2], C Alistair Siebert[1], Guntram Paul[5], Juha T Huiskonen[1], Ian M Jones[4], Robert M Esnouf[1], Elizabeth E Fry[1], Francois F Maree[3,6], Bryan Charleston[2] & David I Stuart[1,7]

Virus capsids are primed for disassembly, yet capsid integrity is key to generating a protective immune response. Foot-and-mouth disease virus (FMDV) capsids comprise identical pentameric protein subunits held together by tenuous noncovalent interactions and are often unstable. Chemically inactivated or recombinant empty capsids, which could form the basis of future vaccines, are even less stable than live virus. Here we devised a computational method to assess the relative stability of protein-protein interfaces and used it to design improved candidate vaccines for two poorly stable, but globally important, serotypes of FMDV: O and SAT2. We used a restrained molecular dynamics strategy to rank mutations predicted to strengthen the pentamer interfaces and applied the results to produce stabilized capsids. Structural analyses and stability assays confirmed the predictions, and vaccinated animals generated improved neutralizing-antibody responses to stabilized particles compared to parental viruses and wild-type capsids.

FMDV is a small-RNA virus whose icosahedral capsid contains 60 copies each of proteins VP1–VP4. FMDV is responsible for a contagious, economically devastating livestock disease endemic in many developing regions of Asia, Africa and South America; developed countries are also at risk of sporadic but serious outbreaks (for example, in the UK in 2001, in Japan in 2010 and in Egypt in 2012 (refs. 1–3)). In areas where FMDV is endemic, disease control is carried out predominantly by vaccination. There are seven serotypes of FMDV (A, O, C, Asia, and Southern African Territories (SAT) 1, 2 and 3)[4], and each contains multiple and constantly evolving subserotype strains. A vaccine against one serotype does not protect against other serotypes or subtypes within a serotype, thus necessitating the continued development of new vaccine strains. The majority of vaccines produced worldwide are type O, whereas SAT2 is the most prevalent serotype in sub-Saharan Africa[5].

FMDV serotypes differ markedly in their capsid stability: A and Asia-1 are relatively stable, whereas O and SAT viruses are more sensitive to heat and pH[6]. Commercial vaccines are produced by chemical inactivation of virus particles, which renders them even less stable, and above 30 °C they rapidly convert into immunogenically incompetent pentameric subunits[6,7]. Thus, vaccine integrity requires expensive, difficult-to-maintain cold chains, and effective protection requires frequent immunizations[5,8]. Recombinant empty capsids show promise as future vaccines because they overcome many of the disadvantages of preparing vaccines from live virus; however, they are even less stable than virus particles[9].

Knowledge of the three-dimensional structure of viral capsids should allow for rational engineering of their properties. Although four different serotypes of FMDV have been analyzed in atomic detail[10–14], few attempts have been made to engineer thermostable capsids[15,16]. The pentameric subassemblies are highly stable, so stabilization of the interpentamer interactions should be sufficient to enhance capsid stability and the effectiveness of vaccine preparations. The introduction of a disulfide bond across the interface between adjacent pentamers has enabled the production of thermostable FMDV empty capsids for an A serotype (A22 Iraq)[17]. However, covalent stabilization may not be compatible with virus viability or with the structure of all viruses[16].

Here, we developed a molecular dynamics (MD)-based strategy for the evaluation of mutations designed to increase capsid stability by increased noncovalent interactions and applied it to the less stable serotypes O and SAT2, and the more stable A viruses. Structural analyses and stability assays confirmed that the method is predictive of increased stability. Furthermore, animals vaccinated with candidate mutant viruses generated improved neutralizing-antibody responses, thus demonstrating potential value for such stabilized vaccine antigens.

RESULTS

FMDV capsids dissociate into pentameric subassemblies

Inactivated FMDV capsids dissociate into pentameric subunits at pH <7.0, at temperatures >30 °C (refs. 1,4,6,15) and after prolonged storage at 4 °C (**Fig. 1a**,**b**). We examined the interface between pentamers for opportunities to stabilize these interpentamer

[1]Division of Structural Biology, University of Oxford, Oxford, UK.
[2]Pirbright Institute, Pirbright, UK.
[3]Transboundary Animal Disease Programme, Agricultural Research Council-Onderstepoort Veterinary Institute, Onderstepoort, South Africa.
[4]Animal and Microbial Sciences, University of Reading, Reading, UK.
[5]Merck Sharp & Dohme Animal Health, Cologne, Germany.
[6]Department of Microbiology and Plant Pathology, University of Pretoria, Pretoria, South Africa.
[7]Diamond Light Source, Didcot, UK. [8]These authors contributed equally to this work. Correspondence should be addressed to D.I.S. (dave@strubi.ox.ac.uk), F.F.M. (mareef@arc.agric.za) or B.C. (bryan.charleston@pirbright.ac.uk).

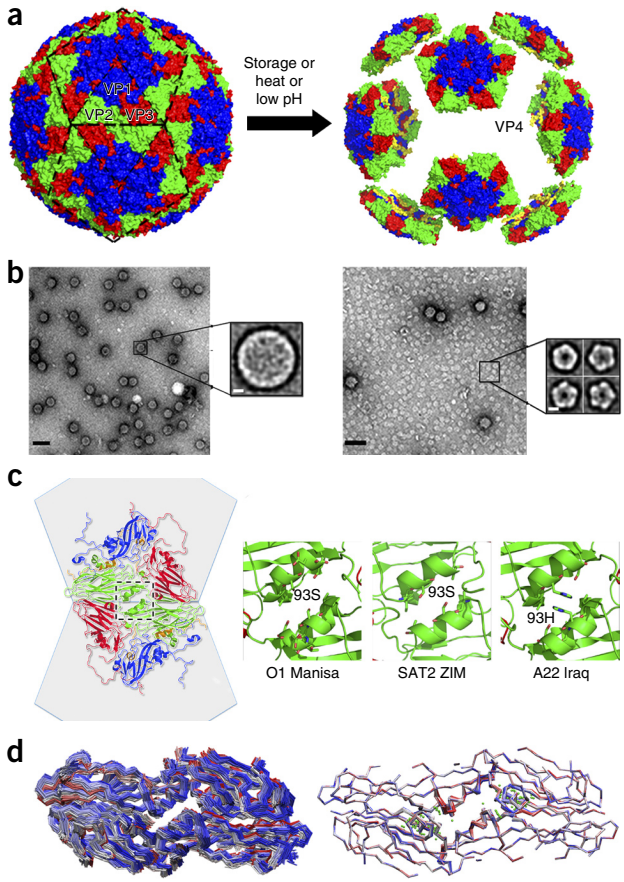

Figure 1 Dissociation of FMDV capsids into pentameric assemblies and design of the models used for MD simulations. (**a**) Surface representation of atomic models of the intact FMDV serotype-O capsid (left, PDB 1BBT) and of its dissociation into 12 pentameric assemblies upon storage, heating or lowering of pH (right). Blue, VP1; green, VP2; red, VP3; yellow, VP4. (**b**) Negative-stain EM images of the inactivated O1M wild-type capsids soon after purification (left, capsids intact with only a few detectable pentamers) or after 10 d of storage at 4 °C (right, 80% dissociated into pentamers). Scale bars, 50 nm. Class averages of the intact capsid or pentamers are shown in zoom view (each calculated from 700 particles with EMAN2 (ref. 38)). Scale bars in zoom view, 5 nm. (**c**) Left, cartoon representation of the atomic structure of the O1M model, showing two icosahedral protomers forming an interpentameric interface. Blue, VP1; green, VP2; red, VP3; yellow, VP4. A truncated model was generated by trimming the protomers to include VP2 and VP3 atoms within 13 Å of the interface, as shown in **d**. Right, residues on two-fold symmetry–related helices for O, A and SAT serotypes. (**d**) 1.5-ns MD trajectory. Left, large r.m.s. deviation from the starting structure for an unrestrained model (average r.m.s. deviation 1.83 Å^2). Right, restrained MD trajectory, with dummy atoms shown in green and placed at the midpoints of the interprotomeric interface to define the restraints. The beginning of the trajectory is shown in red, the middle in white and the end in blue.

contacts by enhancing noncovalent interactions. From four different serotypes[10,11,13,14,18], we identified 85 amino acids contributing to this interface: 57 from VP2 and 28 from VP3. VP2 shows ~80% sequence identity between different serotypes, and we selected nonconserved interface residues inaccessible to antibodies and thus unlikely to affect antigenicity (**Supplementary Fig. 1**) for the introduction of potentially stabilizing interactions (for each residue, a range of mutants was possible). We focused on the region close to the icosahedral two-fold axis because enterovirus uncoating is known to initiate at this point, and disorder of the N terminus of VP2 adjacent to the three-fold axis makes this alternative region less reliable for modeling[19–21].

We chose O1/Manisa/Turkey/69 (O1M), a field strain widely used in current vaccines, and SAT2/ZIM/7/83 (SAT2) as our target antigens, and A22 Iraq 24/64 (A22) as a stable reference strain[17]. In the absence of high-resolution structures, O1BFS (PDB 1BBT)[22] was used as the model for O1M (98% sequence identity in capsid protein VP2), and SAT1 (PDB 2WZR)[14] was used as the model for SAT2 (78% identity in VP2). On the basis of visual inspection of the structures, we generated a panel of 12 potential stabilizing mutants within VP2 for O1M, four of which we also chose for SAT2, and chose the two most promising for A22 (**Table 1**). We modeled these mutants by *in silico* mutagenesis (in COOT[23]) and localized energy minimization.

Table 1 Binding free energy of capsid-stabilizing mutants for O1M, SAT2 and A22

Mutation	O1 Manisa ΔΔ*G* kcal/mol	SAT2 ZIM ΔΔ*G* kcal/mol	A22 Iraq ΔΔ*G* kcal/mol
VP2 93H	−7.7	−5.3	NA
VP2 93Y	−11.8	−12.2	−7.7
VP2 93F	−13.8	−13.2	−10.3
VP2 98F	−10.3	−5.6	–
VP2 97I	−6.8	–	–
VP2 93V	−7.1	–	–
VP2 93L	−1.9	–	–
VP2 93I	−7.2	–	–
VP2 93M	−2.8	–	–
VP2 93W	−9.5	–	–
VP2 97Q	−5.5	–	–
VP2 90N	−3.5	–	–
Negative controls			
VP2 60G	+33.7		
VP2 60L	+24.0		
VP2 57E	+17.7		
VP2 57L	+12.3		

NA, not applicable.

MD simulations and binding free-energy calculations

We devised a new MD-simulation protocol for rapid evaluation of the relative stability potential of mutant viruses. Atomistic dynamics is usually applied to complete biological ensembles[24,25]; however, in the context of small, well-defined changes in a complex virus particle, this approach has a poor signal-to-noise ratio and is expensive computationally. We therefore decreased the complexity of the simulation, initially to two interfacial protomers (**Fig. 1c**), which required a week of processing on eight central-processing-unit cores (AMD Opteron 6174 at 2.2 GHz). Nonetheless, artifacts made it difficult to detect small changes in the binding free energy of the interface. Therefore we devised a protocol in which the model was further trimmed to atoms within 13 Å of the interface, and positional restraints that increased with distance from the interface were applied. To enable this, we placed nonphysical 'dummy' atoms midway between pairs of interacting atoms along the contact interface centered on the icosahedral two-fold axis of symmetry. During simulations, we defined restraints such that atoms within 10 Å of any dummy atom were allowed to move freely, whereas atoms that were more remote, and the dummy atoms themselves, were tightly restrained (**Fig. 1d**). These restraints considerably simplified the simulation (~24 h computation with the same AMD central processing units) and dramatically reduced the noise by 'freezing' unchanged parts of the structure, including the disconnected atoms at the periphery of

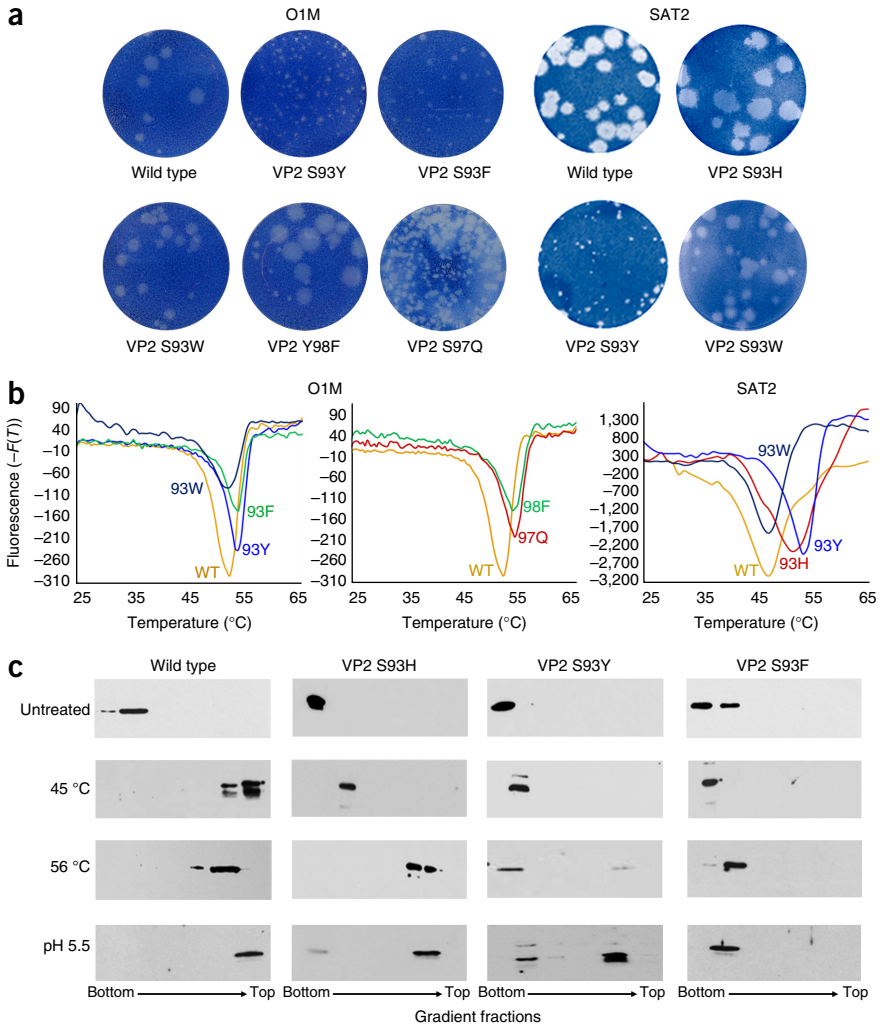

Figure 2 Growth characteristics and stability of the engineered capsids. (**a**) Plaques formed in BHK-21 cells by wild-type and mutant O1M and SAT2 viruses. The patterns of CPE correlated with plaque size. (**b**) Fluorescence assay measuring thermostability of infectious O1M viruses (left and middle) and inactivated SAT2 viruses (right) at pH 7.5 (ref. 29). *F*, fluorescence; *T*, temperature. Wild-type O1M and SAT2 dissociated at 52.0 °C and 47.0 °C, respectively. Mutant S93Y dissociated at 53.5 °C for both O1M and SAT2. O1M mutants S93F, S97Q and Y98F dissociated at 53.5 °C, 54.0 °C and 53.5 °C, respectively. Mutant S93H (SAT2) dissociated at 51.0 °C. S93W dissociation was similar to that of parental virus in both O1M and SAT2. (**c**) Thermostability and pH stability of the recombinant empty capsids assayed by western blotting after sedimentation through 15–45% sucrose density gradients, in which dissociated capsids remain at the top of the gradient, and intact capsids migrate to the bottom. Fractions were probed with anti–FMDV O1M polyclonal antibodies recognizing VP1 (refs. 39,40) (ELISA data are shown in **Supplementary Fig. 3**; uncropped gels are shown in **Supplementary Data Set 1**).

the model. We tested a set of negative controls with the O1M model to validate the protocol, whereby a salt-bridge or hydrogen-bond network was deliberately disrupted (**Table 1**); these mutations resulted in positive $\Delta\Delta G$ values. In one simulation, VP2 Arg60, which forms the salt bridge with the VP2 Glu212 on the opposite protomer, was substituted with either glycine or leucine; as expected, in both cases the interface was destabilized. Similarly, when Gln57, which makes a network of hydrogen bonds across the interface, was substituted with glutamate or leucine, an unstable interface was generated. However, such dynamics-based methods cannot model additional covalent interactions, such as disulfide bonds.

Putative mutations that confer increased stability

The results of the free-energy calculations are shown in **Table 1**. Residue 93 of VP2 is part of an α-helix adjacent to the icosahedral two-fold axis and is largely conserved within but not between serotypes (**Supplementary Fig. 1** and **Fig. 1c**). The relatively stable A serotype has a histidine at this position, whose imidazole ring forms a hydrophobic stacking interaction with the corresponding symmetry-related moiety. Simulation results suggested that this virus could be further stabilized by mutation to tyrosine or, more preferably, to phenylalanine. For O1M and SAT2, the simulations suggested that stability would be enhanced by mutation of the equivalent serine to histidine (S93H) and would be further improved by mutation to tyrosine, whose side chain was predicted to hydrogen-bond to the backbone of VP2 89. Nonetheless, a phenylalanine was predicted to confer even greater stability. Substitution with a bulky tryptophan was less effective, as were residues with nonaromatic hydrophobic side chains (valine, leucine, isoleucine and methionine) (**Table 1**). Some VP2 mutations away from the two-fold axis produced stabilization (S97Q, S97I and to a lesser extent V90N), and Y98F was predicted to be most effective.

Mutant viruses are infectious and stable

The effects of the amino acid mutations were first tested in recombinant virus. Transcripts were electroporated or transfected into BHK-21 cells to generate infectious stocks. These stocks were then used to infect ZZ-R127 goat epithelial cells, which are highly susceptible to FMDV infection[26]. Subsequent passages in BHK-21 cells, which are commonly used in the production of FMD vaccines, were possible because the SAT2 virus was cell-culture adapted, whereas two VP3 mutations (H56R and D60G) were introduced in O1M, thus enabling cell entry via heparan sulfate[27]. These mutations, remote from the pentamer interface, did not affect the particle stability (**Supplementary Fig. 1**) and are often present in vaccine strains. All recombinant viruses were sequenced after four passages, and the results revealed no changes or obvious subpopulations. All produced clear, consistent, cytopathic effects (CPE); however, we observed differences between viruses. The patterns of CPE and plaque sizes varied markedly, and in general stabilized viruses yielded substantially smaller plaques than the parental viruses (**Fig. 2a**). However, the yields of wild-type and mutant viruses were broadly similar (**Supplementary Table 1**). In addition to generating recombinant viruses, we made recombinant empty capsids containing the same amino acid substitutions by using mammalian- and insect-cell expression systems described previously[17,28].

We determined capsid stability by fluorescence thermal stability assays[29] at pH 7.5. For O1M, wild-type virus dissociated at 52.0 °C,

Table 2 Data collection and refinement statistics

	O1M VP2 S93Y[a]	A22 VP2 H93F[b]
Data collection		
Space group	*I*23	*I*222
Cell dimensions		
a, *b*, *c* (Å)	344.08, 344.08, 344.08	327.6, 341.3 363.6
α, β, γ (°)	90, 90, 90	90, 90, 90
Resolution (Å)[c]	46.0–3.5 (3.56–3.5)	50.0–2.4 (2.49 –2.4)
R_{merge}	0.46	0.27
$I / \sigma I$	1.7 (0.76)	1.23 (0.5)
Completeness (%)	77.7 (71.1)	45.5 (39.8)
Redundancy	1.5 (1.4)	1.4 (1.3)
Refinement		
Resolution (Å)	46.0–3.5	50.0–2.4
No. reflections	65,915	347,924
R_{work} / R_{free}	36.35 / –	20.6 / 21.2
No. atoms		
Protein	5,149	5,192
Ligand/ion	–	–
Water	0	196
B factors		
Protein	49.2	27.0
Ligand/ion	–	–
Water	–	30.6
r.m.s. deviations		
Bond lengths (Å)	0.011	0.013
Bond angles (°)	1.816	1.716

[a]The data for O1M VP2 S93Y were collected from 14 different crystals. [b]The data for A22 VP2 H83F were collected from 19 different crystals. [c]Values in parentheses are for highest-resolution shell.

and S93W dissociated similarly, whereas S93Y, S93F and Y98F dissociated at 53.5 °C. Inactivated SAT2 followed a similar pattern: wild-type and S93W capsids dissociated at a similar temperature (47.0 °C), whereas S93H and S93Y dissociated at 51.0 °C and 53.5 °C, respectively (**Fig. 2b** and **Supplementary Table 2**). At lower pH (6.5), wild-type O1M capsids dissociated at 31.0 °C, whereas mutant capsids were more stable; S93W dissociated at 34.0 °C, S98F and S97Q at 35.0 °C, and S93Y and S93F at 38.0 °C (**Supplementary Fig. 1**).

We assessed the stability of inactivated wild-type and S93Y O1M particles by negative-stain EM. Immediately after purification, ~90% of wild-type capsids were intact compared to almost 100% for S93Y (on the basis of the mean particle count within five randomly selected areas of the grid). After 10 d of storage at 4 °C, only ~20% of the wild-type capsids remained intact, compared to 90% for the mutant (**Supplementary Fig. 2**). Finally, we incubated samples at 37 °C for 5, 10 or 20 min and analyzed them by EM. Remarkably, only ~5% of the wild-type virions remained intact, compared to ~60% for the mutant after 20-min incubation at 37 °C (**Supplementary Fig. 2**). An ELISA on infectious O1M virus produced similar results. We incubated wild-type or S93Y particles at 37 °C for up to 72 h and analyzed samples with llama antibodies (VHH M170, which recognizes intact capsids, and VHH M3, which recognizes pentamers)[30]. As expected, more than 50% of the S93Y capsids were intact after 72 h versus only 15% of the wild type (**Supplementary Fig. 2**). In conclusion, the mutant viruses were consistently more stable at elevated temperatures and at low pH, and the results correlated well with the MD simulations.

Stability of recombinant empty capsids

For empty particles, the RNA fluorescence assay could not be used, so we performed analysis by fractionation on sucrose density gradients and subsequent western blotting. We heated purified wild-type and mutant (S93H, S93Y and S93F) O1M capsids at 45 °C for 1 h. The mutant empty capsids sedimented similarly to intact particles, whereas wild-type empty capsid material stayed near the top of the gradient, thus confirming dissociation (**Fig. 2c** and **Supplementary Fig. 3**). In a more extreme test, we incubated the mutant capsids at 56 °C for 2 h before analysis. Mutant S93H was unstable, S93Y was partially stable (~25% dissociated particles as estimated visually), and S93F was completely stable. As visualized by EM, the peak fraction of heat-treated S93F revealed mostly intact capsids, with few pentamers (**Supplementary Fig. 4**). We obtained similar results with A22 empty capsids: the H93F mutant remained intact after 2 h at 56 °C, whereas wild-type capsids completely dissociated (**Supplementary Fig. 5**). To study the effect of storage at moderate temperature on empty capsids, we incubated O1M wild type and

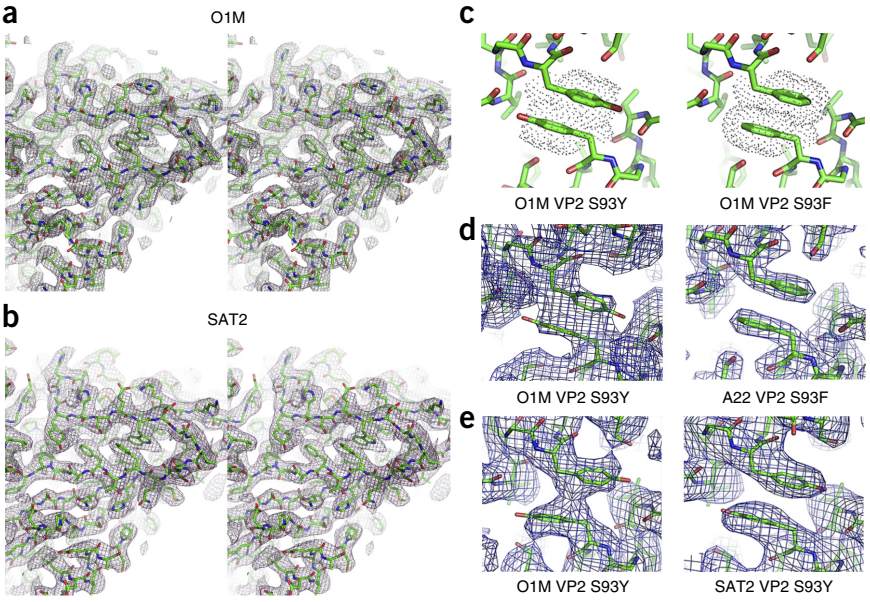

Figure 3 Structural analysis of stable engineered capsids. The structures of engineered mutants O1M S93Y, A22 H93F and SAT2 S93Y were determined by X-ray crystallography and cryo-EM. (**a**,**b**) Stereo views of the density from cryo-EM reconstructions for O1M S93Y at 3.2 Å (**a**) and SAT2 S93Y at 3.5 Å (**b**). The quality of the cryo-EM density maps allowed unambiguous fitting and refinement of the major capsid proteins. (**c**) Predicted structures showing the stacking interactions of tyrosine and phenylalanine at position 93 of O1M VP2 proteins on the two-fold symmetry axis. (**d**) X-ray structures of O1M S93Y and A22 H93F at 3.5-Å and 2.4-Å resolution, respectively. The electron density map clearly showed a stacking interaction of phenylalanine side chains for A22 H93F. Tyrosine density for O1M S93Y was observable but less well defined because of the twinning of O1M crystals. (**e**) Cryo-EM maps showing the density for S93Y for O1M and SAT2 at 3.2-Å and 3.5-Å resolution, respectively.

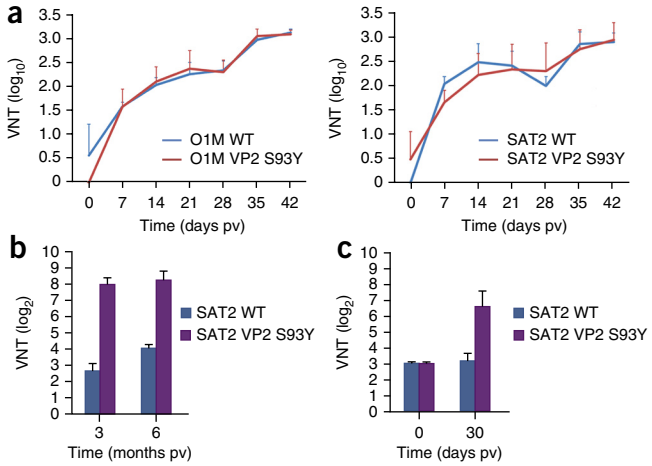

Figure 4 Immunogenicity of inactivated wild-type and stabilized viruses. (**a**) Mean virus neutralizing-antibody titer (VNT (log_{10})) of calves vaccinated with purified inactivated virus of the O1M (left) and SAT2 (right) serotypes. Groups of four calves were vaccinated with either wild-type or mutant S93Y at days 0 and 28; blood samples were assayed at 0, 7, 14, 21, 28, 35 and 42 days pv, error bars, s.d. (**b**) VNTs of guinea pigs to assess immunogenicity of inactivated particles after 1 month of long-term storage. Before immunization, formulated vaccines were stored for 1 month at 4 °C. Two groups of ten guinea pigs were each immunized with either wild-type or S93Y SAT2 antigen, and VNTs were assessed at 3 and 6 months pv. Error bars, s.d. (**c**) VNTs of guinea pigs to assess immunogenicity of inactivated particles after 6 months of long-term storage, showing protective VNTs for only stabilized antigen. Equivalent aliquots of wild-type and stabilized SAT2 vaccines were stored for 6 months at 4 °C before inoculation of two groups of ten guinea pigs. Error bars, s.d.

S93F mutant for 24 h or 96 h at 37 °C. Wild-type capsids dissociated, whereas S93F capsids remained intact (**Supplementary Fig. 6**). To determine pH stability, we incubated O1M capsids at pH 5.5 for 15 min. Wild-type capsids dissociated completely, whereas S93H and S93Y capsids were partially stable (25% remained intact), and S93F remained completely intact (**Fig. 2c**).

Structure analysis of stabilized capsids

We determined structures of the stabilized capsids by X-ray crystallography and cryo-EM. SAT2 crystals did not diffract to high resolution; however, we solved structures of the mutant A22 empty capsid and mutant O1M virus at 2.4-Å and 3.5-Å resolution, respectively, using *in situ* room-temperature X-ray crystallography[17,31]. The O1M crystals were merohedrally twinned, and we developed a protocol to deconvolute the twinned reflections[32] (H.M.G., unpublished data). Refinement using strict noncrystallographic symmetry and real-space averaging yielded reliable maps and models for both structures (**Table 2**). The refined atomic models were very similar to those of the respective natural empty particles and parental viruses[10–12,17], except that, as predicted, the aromatic side chains of VP2 residue 93 stacked at the two-fold axes.

Owing to the lower quality of the O1M analysis, and our inability to obtain diffraction-quality crystals of SAT2 particles, we determined the structures of inactivated O1M S93Y and SAT2 S93Y by cryo-EM (Online Methods). 8,267 particles of O1M and 8,156 particles of SAT2 yielded structures at 3.2- and 3.5-Å resolution (Fourier shell correlation of 0.143), respectively (**Fig. 3a**,**b**, **Supplementary Fig. 7** and **Supplementary Table 3**). We compared the predicted and experimental stacking of the tyrosine and phenylalanine side chains around the two-fold axis in the X-ray and cryo-EM structures (**Fig. 3c**–**e**).

Immunogenicity of stabilized mutants

To compare the immunogenicity of wild-type and stabilized viruses, we vaccinated calves with purified inactivated wild-type or mutant (S93Y) virus of both the O1M and SAT2 serotypes. We maintained inactivated antigen at 4 °C and purified it immediately before use. We measured serum virus neutralization antibody titers (VNTs) at different times postvaccination (pv) (**Fig. 4a**). In all animals, we observed high VNTs on day 28 at the time of boost immunization (mean antibody titers >2 log_{10}, which is considered protective[33]); titers were substantially increased (>3 log_{10}) by day 42 pv.

Because mutant and wild-type antigens had equivalent immunogenic properties when administered directly after purification, we compared their immunogenicity after long-term storage. For this, we stored inactivated wild-type and mutant S93Y FMDV SAT2 particles at doses of 10 μg each, formulated as described above, for 1 month at 4 °C and used them to vaccinate two groups of ten guinea pigs. We assessed VNTs at 3 and 6 months pv (**Fig. 4b**). At 3 months pv, we observed substantially higher VNTs in animals vaccinated with the stabilized SAT2 antigen (>8 log_2 considered protective[34]) than in animals vaccinated with the wild-type SAT2 antigen (<3 log_2). At 6 months pv, the group mean VNT in animals immunized with the stabilized SAT2 antigen remained at >8 log_2, whereas wild type–immunized animals' antibody titers remained below protective levels. Thus, the stabilized vaccine performed markedly better than the wild-type vaccine.

In a further iteration, we stored equivalent aliquots of wild-type and stabilized vaccines for 6 months at 4 °C and again used them to immunize two groups of ten guinea pigs. No animal had a VNT titer at day 0, but by day 30 pv, although the mean VNT titer of the group inoculated with wild-type vaccine remained low (~3 log_2), the mean titer of the group inoculated with stabilized virus was markedly higher and was consistent with protection, >6 log_2 (**Fig. 4c**). Thus, only stabilized particles were able to induce VNT titers, a result consistent with protection after 1 month or 6 months of storage at 4 °C.

DISCUSSION

FMDV vaccines with higher stability have the potential to be more effective. However, very few natural FMDV variants with increased resistance to heat or pH[35,36] have been reported, possibly because overstabilization hinders the release of the viral genome during cell entry. We therefore investigated the rational introduction of mutations to increase thermostability, earlier attempts at which have had only marginal success[16]. We have previously reported a stable disulfide bond at the icosahedral two-fold axis between adjacent pentamers in the A22 virus, thus allowing the production of thermostable and pH-stable recombinant empty particles[17]. Because covalent modification was unlikely to be suitable with engineered viruses and may not be generally applicable, we devised a strategy that allows general mutations conferring noncovalent stabilization to be evaluated *in silico*. We exploited highly restrained atomistic MD simulations focused on the appropriate part of the complete virion to efficiently and reliably calculate the changes in binding free energy for interactions between adjacent pentamers within the FMDV capsid, thus allowing screening and ranking of candidate mutations. We found that a single-residue mutation generating hydrophobic stacking of aromatic side chains at the two-fold axis between adjacent pentamers (position 93 of VP2) was effective in stabilizing the particle, results echoing those from studies in enteroviruses that identify the place at which the particle opens up to start uncoating[20,21]. The predicted degree of stabilization correlated with

hydrophobicity, thus with O1M, S93H ($\Delta\Delta G$ = −7.7 kcal/mol) < S93Y ($\Delta\Delta G$ = −11.8 kcal/mol) < S93F ($\Delta\Delta G$ = −13.8 kcal/mol). Similarly, when the equivalent (histidine) residue of the stable A serotype, A22 Iraq, was substituted by tyrosine ($\Delta\Delta G$ = −7.7 kcal/mol) or phenylalanine ($\Delta\Delta G$ = −10.3 kcal/mol), the stability of the interface was further increased.

Engineering the stabilization mutations decreased the plaque sizes for both O1M and SAT2 viruses, possibly by delaying viral genome release. Both infectious viruses and recombinant empty capsids carrying these mutations were indeed thermostable and pH stable, and the degree of stabilization mirrored the *in silico* calculations. This noncovalent stabilization of two particularly unstable serotypes produced particles of similar stability to that of covalently cross-linked A22 particles[17]. Formulated vaccines from inactivated wild-type and stabilized O and SAT2 viruses produced equivalent protective levels of neutralizing antibodies in cattle, thus demonstrating the immunogenicity of the engineered particles. The stabilized inactivated vaccine antigen was also intact after 96 h at 37 °C and is expected to be more tolerant of suboptimal cold-chain performance; goals for the stability of SAT2 have been described by Anderson *et al.*[37]. Furthermore, after storage for 1 or 6 months at 4 °C, stabilized particles produced substantially higher VNTs in guinea pigs than did wild-type particles, commensurately with an increase in vaccine shelf life.

In conclusion, we have devised a new restrained MD protocol to drive structure-based design of stabilized FMDV viruses and empty capsids. Such new effective FMDV vaccines would, in the context of empty capsids, eliminate the considerable risks involved in producing vaccine from infectious virus. This strategy may be relevant to many other picornaviruses that are responsible for causing a wide range of mild–to–life-threatening diseases affecting humans and other animals.

Accession codes. Coordinates and structure factors for the inactivated O1M and A22 mutant particles have been deposited in the Protein Data Bank under accession codes 5DDJ and 5D8A, respectively. The EM structures for O1M and SAT2 mutant particles have been deposited in the Protein Data Bank under accession codes 5AC9 and 5ACA, respectively, and in the EM Data Bank under accession codes 3129 and 3130, respectively.

ACKNOWLEDGMENTS

We thank the World Reference Laboratory for VNT determination; beamline staff at the Diamond Light Source for assistance; J. Dong and J. Diprose for computing support; P. Afonine and G. Murshudov for advice on Phenix and Refmac; K. Harlos and T. Walter for help with crystallography; D. Goovaerts and E. Rieder for helpful discussions; and B. Haas (Friedrich-Loeffler-Institut) for providing ZZ_R 127 cells. We are grateful to the Wellcome Trust (WT) for a Translation Award to fund this work (grant no. 089755 to B.C., E.E.F., T.J. and F.F.M.). T.J. and B.C. were funded by the Biotechnology and Biological Sciences Research Council Institute Strategic Programme on Livestock Viral Diseases at The Pirbright Institute. The Oxford Particle Imaging Centre electron microscopy facility was founded by a WT Joint Infrastructure Fund award (060208/Z/00/Z to D.I.S.) and is supported by a WT equipment grant (093305/Z/10/Z to K. Grünewald). The WT, UK Medical Research Council (MRC) and Biotechnology and Biology Research Council also support the National EM facility, which provided the K2 detector. B.C. and D.I.S. are supported as Jenner investigators, J.R. and A.K. are WT supported, and E.E.F. and D.I.S. are supported by the UK MRC (grant no. G100099 to D.I.S.). The work of the WT Centre in Oxford is supported by the WT core award 090532/Z/09/Z.

AUTHOR CONTRIBUTIONS

A.K., E.E.F., R.M.E. and D.I.S. developed MD-simulation protocols; A.K., J.S., K.S., A.B., S.L. and C.P. prepared samples; J.R., H.M.G., J.T.H., E.P.-M., G.P., C.A.S., F.F.M. and E.E.F. assisted in research; A.K., J.S., F.F.M., E.E.F., T.J., I.M.J., R.M.E., D.I.S. and B.C. designed the study; all authors analyzed data; and A.K., J.S., E.E.F., B.C. and D.I.S. wrote the manuscript.

References

1. Grubman, M.J. & Baxt, B. Foot-and-mouth disease. *Clin. Microbiol. Rev.* **17**, 465–493 (2004).
2. Muroga, N. *et al.* The 2010 foot-and-mouth disease epidemic in Japan. *J. Vet. Med. Sci.* **74**, 399–404 (2012).
3. Kandeil, A. *et al.* Characterization of the recent outbreak of foot-and-mouth disease virus serotype SAT2 in Egypt. *Arch. Virol.* **158**, 619–627 (2013).
4. Bachrach, H.L. Foot-and-mouth disease. *Annu. Rev. Microbiol.* **22**, 201–244 (1968).
5. Doel, T.R. FMD vaccines. *Virus Res.* **91**, 81–99 (2003).
6. Doel, T.R. & Baccarini, P.J. Thermal stability of foot-and-mouth disease virus. *Arch. Virol.* **70**, 21–32 (1981).
7. Doel, T.R. & Chong, W.K.T. Comparative immunogenicity of 146S, 75S and 12S particles of foot-and-mouth disease virus. *Arch. Virol.* **73**, 185–191 (1982).
8. Hall, M.D., Knowles, N.J., Wadsworth, J., Rambaut, A. & Woolhouse, M.E.J. Reconstructing geographical movements and host species transitions of foot-and-mouth disease virus serotype SAT 2. *MBio* **4**, e00591–13 (2013).
9. Basavappa, R. *et al.* Role and mechanism of the maturation cleavage of VP0 in poliovirus assembly: structure of the empty capsid assembly intermediate at 2.9 Å resolution. *Protein Sci.* **3**, 1651–1669 (1994).
10. Acharya, R. *et al.* The three-dimensional structure of foot-and-mouth disease virus at 2.9 A resolution. *Nature* **337**, 709–716 (1989).
11. Curry, S. *et al.* Perturbations in the surface structure of A22 Iraq foot-and-mouth disease virus accompanying coupled changes in host cell specificity and antigenicity. *Structure* **4**, 135–145 (1996).
12. Curry, S. *et al.* Dissecting the roles of VP0 cleavage and RNA packaging in picornavirus capsid stabilization: the structure of empty capsids of foot-and-mouth disease virus. *J. Virol.* **71**, 9743–9752 (1997).
13. Lea, S. *et al.* The structure and antigenicity of a type C foot-and-mouth disease virus. *Structure* **2**, 123–139 (1994).
14. Reeve, R. *et al.* Sequence-based prediction for vaccine strain selection and identification of antigenic variability in foot-and-mouth disease virus. *PLoS Comput. Biol.* **6**, e1001027 (2010).
15. Ellard, F.M., Drew, J., Blakemore, W.E., Stuart, D.I. & King, A.M. Evidence for the role of His-142 of protein 1C in the acid-induced disassembly of foot-and-mouth disease virus capsids. *J. Gen. Virol.* **80**, 1911–1918 (1999).
16. Mateo, R., Luna, E., Rincón, V. & Mateu, M.G. Engineering viable foot-and-mouth disease viruses with increased thermostability as a step in the development of improved vaccines. *J. Virol.* **82**, 12232–12240 (2008).
17. Porta, C. *et al.* Rational engineering of recombinant picornavirus capsids to produce safe, protective vaccine antigen. *PLoS Pathog.* **9**, e1003255 (2013).
18. Berman, H.M. *et al.* The Protein Data Bank. *Nucleic Acids Res.* **28**, 235–242 (2000).
19. Wang, X. *et al.* A sensor-adaptor mechanism for enterovirus uncoating from structures of EV71. *Nat. Struct. Mol. Biol.* **19**, 424–429 (2012).
20. Ren, J. *et al.* Picornavirus uncoating intermediate captured in atomic detail. *Nat. Commun.* **4**, 1929 (2013).
21. Butan, C., Filman, D.J. & Hogle, J.M. Cryo-electron microscopy reconstruction shows poliovirus 135S particles poised for membrane interaction and RNA release. *J. Virol.* **88**, 1758–1770 (2014).
22. Fry, E., Acharya, R. & Stuart, D. Methods used in the structure determination of foot-and-mouth disease virus. *Acta Crystallogr. A* **49**, 45–55 (1993).
23. Emsley, P. & Cowtan, K. Coot: model-building tools for molecular graphics. *Acta Crystallogr. D Biol. Crystallogr.* **60**, 2126–2132 (2004).
24. Karplus, M. & McCammon, J.A. Molecular dynamics simulations of biomolecules. *Nat. Struct. Biol.* **9**, 646–652 (2002).
25. Klepeis, J.L., Lindorff-Larsen, K., Dror, R.O. & Shaw, D.E. Long-timescale molecular dynamics simulations of protein structure and function. *Curr. Opin. Struct. Biol.* **19**, 120–127 (2009).
26. Jackson, T., Sheppard, D., Denyer, M., Blakemore, W. & King, A.M. The epithelial integrin αvβ6 is a receptor for foot-and-mouth disease virus. *J. Virol.* **74**, 4949–4956 (2000).
27. Fry, E.E. *et al.* The structure and function of a foot-and-mouth disease virus-oligosaccharide receptor complex. *EMBO J.* **18**, 543–554 (1999).
28. Porta, C. *et al.* Efficient production of foot-and-mouth disease virus empty capsids in insect cells following down regulation of 3C protease activity. *J. Virol. Methods* **187**, 406–412 (2013).

29. Walter, T.S. *et al.* A plate-based high-throughput assay for virus stability and vaccine formulation. *J. Virol. Methods* **185**, 166–170 (2012).
30. Harmsen, M.M., Fijten, H.P., Westra, D.F. & Coco-Martin, J.M. Effect of thiomersal on dissociation of intact (146S) foot-and-mouth disease virions into 12S particles as assessed by novel ELISAs specific for either 146S or 12S particles. *Vaccine* **29**, 2682–2690 (2011).
31. Axford, D. *et al. In situ* macromolecular crystallography using microbeams. *Acta Crystallogr. D Biol. Crystallogr.* **68**, 592–600 (2012).
32. Lea, S. & Stuart, D. Deconvolution of fully overlapped reflections from crystals of foot-and-mouth disease virus O1 G67. *Acta Crystallogr. D Biol. Crystallogr.* **51**, 160–167 (1995).
33. Barnett, P.V., Statham, R.J., Vosloo, W. & Haydon, D.T. Foot-and-mouth disease vaccine potency testing: determination and statistical validation of a model using a serological approach. *Vaccine* **21**, 3240–3248 (2003).
34. Bolwell, C., Parry, N.R. & Rowlands, D.J. Comparison between *in vitro* neutralization titres and *in vivo* protection against homologous and heterologous challenge induced by vaccines prepared from two serologically distinct variants of foot-and-mouth disease virus, serotype A22. *J. Gen. Virol.* **73**, 727–731 (1992).
35. Martín-Acebes, M.A., Rincon, V., Armas-Portela, R., Mateu, M.G. & Sobrino, F. A single amino acid substitution in the capsid of foot-and-mouth disease virus can increase acid lability and confer resistance to acid-dependent uncoating inhibition. *J. Virol.* **84**, 2902–2912 (2010).
36. Mateo, R., Luna, E. & Mateu, M.G. Thermostable variants are not generally represented in foot-and-mouth disease virus quasispecies. *J. Gen. Virol.* **88**, 859–864 (2007).
37. Anderson, E.C., Doughty, W.J. & Spooner, P.R. Variation in the thermal stability of isolates of foot-and-mouth disease type SAT 2 and its significance in the selection of vaccine strains. *J. Comp. Pathol.* **92**, 495–507 (1982).
38. Tang, G. *et al.* EMAN2: an extensible image processing suite for electron microscopy. *J. Struct. Biol.* **157**, 38–46 (2007).
39. Ferris, N.P. *et al.* Utility of recombinant integrin αvβ6 as a capture reagent in immunoassays for the diagnosis of foot-and-mouth disease. *J. Virol. Methods* **127**, 69–79 (2005).
40. Ferris, N.P. & Donaldson, A.I. Serological response of guinea pigs to inactivated 146S antigens of foot and mouth disease virus after single or repeated inoculations. *Rev. Sci. Tech. Off. Int. Epiz* **3**, 563–574 (1984).

ONLINE METHODS

Molecular dynamics methods. These are described in the **Supplementary Note**.

Generation of infectious recombinant cDNA. Infectious FMDV O1K/O1 Manisa (O1M) chimeric clones were constructed with reverse genetics. Briefly, cDNA encoding the VP2, VP3, VP1 and 2A proteins was removed from a derivative of the pT7S3 O1K infectious clone, termed pT7SBmuts, leaving cDNA encoding the Lpro, VP4, 2B, 2C, 3A, 3B, 3C and 3D proteins[41]. The removed cDNA was replaced with the corresponding O1M cDNA from pGEM9zf subclones, encoding the wild-type or a specific amino acid substitution within the VP2 structural protein[42] (UKG/35/2001; GenBank AJ539141). The encoded amino acid substitutions within VP2 were generated with the QuikChange Lightning Mutagenesis kit (Agilent Technologies) according to the manufacturer's instructions. For SAT2, the leader-P1-2A coding region of pSAT2 (ref. 43) was cloned into pBS (Stratagene) with EcoRI and XmaI restriction-enzyme sites. Site-directed mutagenesis was performed with the QuikChange Site-Directed Mutagenesis kit (Stratagene). The pSAT2/pBS clones containing the desired mutations, as verified by nucleotide sequencing, were digested with SspI and XmaI to recover the mutant leader-P1-2A region, which was cloned back into the pSAT2 genetic backbone. All mutations were verified by sequencing.

Preparation of infectious RNA, electroporation and transfection. RNA was transcribed from the infectious clones with the MEGAscript T7 kit (Invitrogen). Infectious RNA was electroporated with a Bio-Rad Gene Pulser (two pulses at 0.75 kV and 25 mF) or transfected into BHK-21 cells (clone 13). After 24 h, the cells were frozen and then thawed in their growth medium. After clarification by centrifugation, the supernatant containing the initial virus stock (termed 'passage 0', P0) was harvested. Fetal goat tongue (ZZ-R 127) or BHK-21 cells were subsequently used to passage the viruses[44]. Cells were infected for 24 h between passages. The yields of wild-type and mutant viruses were similar. BHK-21 cells (clone 13) have been maintained in the Pirbright Institute since 1965. ZZ_R 127 cells were a gift from B. Haas (Friedrich-Loeffler-Institut, (FLI)). All cell cultures were free of mycoplasma and bovine viral diarrhea virus.

Genome amplification and sequencing. Total RNA was extracted with TRIzol (Invitrogen), and the viral RNA genome was reverse-transcribed and PCR-amplified with a One-Step RT-PCR kit (Qiagen). Sequencing reactions were performed with an aliquot of the purified PCR product and the BIG Dye Terminator v3.1 cycle sequencing kit (Applied Biosystems).

Plaque assay. Confluent monolayers of goat epithelial cells or BHK-21 cells were infected with serial dilutions of virus stocks, overlaid with indubiose (Pall Life Sciences) and incubated for 24–48 h at 37 °C. Cells were fixed and stained (4% formaldehyde in PBS containing methylene blue), and the overlay was removed[26]. The diameters of 50 parental (wild-type) plaques were measured with a microscope eyepiece micrometer. These were averaged, defined as 100%, and compared against 50 mutant plaque diameters.

Virus titers. Virus titers were estimated by plaque assays. For O1M, confluent monolayers of BHK-21 cells were infected with serial dilutions of FMDV virus stocks in triplicate, overlaid with indubiose and incubated for 24–48 h at 37 °C. The cells were then fixed and stained (4% formaldehyde in PBS containing methylene blue) before removal of the overlay[26]. For SAT2, BHK-21 cells were infected for 1 h; this was followed by the addition of 2 ml tragacanth overlay[45]. After incubation at 37 °C for 48 h, the infected monolayers were stained with 1% (w/v) methylene blue in 10% (v/v) ethanol and 10% (v/v) formaldehyde in PBS, pH 7.4.

Virus inactivation. Chemical inactivation followed standard operating procedures (SOPs) in line with disease security regulations at The Pirbright Institute. Upon CPE, the cell-culture medium, containing the virus, was harvested and clarified by centrifugation at 2,095*g* for 30 min at 4 °C. Clarified supernatant was inactivated by two consecutive incubations with binary ethyleneimine (BEI). A 10-ml aliquot of 0.1 M BEI solution was added to every 1,000 ml of virus harvested (to yield a final BEI concentration of 0.001 M); this was followed by incubation for 24 h at 37 °C. During incubation, the virus/BEI solutions were mixed by periodic inversion. Innocuity tests were performed by the World Reference Laboratory (WRL) at The Pirbright Institute.

Generation of recombinant empty particles. Expression of recombinant empty capsids used two different systems: O1M capsids were produced with a vaccinia virus (VV) mammalian-cell expression system, and A22 capsids were produced with a baculovirus (BV) insect-cell expression system according to previously described methodology[17]. Briefly, for VV expression cassettes containing synthetic cDNA encoding VP0, VP3 and VP1 and the 2A and 3C nonstructural proteins of wild-type FMDV were synthesized (GeneArt) and cloned into a VV vector, pBG200. Recombinant viruses were generated by transfecting the pBG200 vector into simian kidney-derived CV-1 cells that had been infected with VV. Recombinant VVs (VV-FMDV) were selected by plaque assay and verified by PCR with FMDV-specific primers. FMDV empty capsids were amplified in RK13 or HEK293 cells after dual infection with a recombinant VV expressing T7 polymerase (VV-T7) as previously described[17]. For insect-cell expression, the pTri-EX–derived plasmid pOPINE[46] was used to generate recombinant BVs encoding the FMDV proteins. The pOPINE vector containing the FMDV coding sequence and the AcMNPV (*Autographa californica* nucleopolyhedrovirus) FlashBacGold DNA (from Oxford Expression Technologies) were transfected into Sf9 insect cells (*Spodoptera frugiperda*) with Lipofectin. Recombinant AcMNPV was harvested from supernatant 5 d after infection (P0 virus stock) and amplified by infection of Sf9 cells at 50% confluency with 200 µl recombinant virus per 175 cm^2 flask and collection of the supernatant after 5 d (P1 virus stock). Recombinant empty capsids were expressed by infection of Sf9 cells ($1–2 \times 10^6$/ml) with 1/10 volume of the P1 BV stock. Mutants were generated by PCR mutagenesis (QuikChange Lightning Mutagenesis Kit, Agilent Technologies) according to the manufacturer's instructions. CV-1, RK13 and HEK 293 cells were sourced from the European Collection of Cell Cultures (ECACC). All cell cultures were free of mycoplasma and bovine viral diarrhea virus. Sf9 insect cells were obtained from Sigma-Aldrich.

Purification of viruses. Frozen lysates containing inactivated antigens were thawed on ice and clarified by centrifugation at 3,500*g* for 30 min at 4 °C. Virus was then precipitated by the addition of either 30% w/v ammonium sulfate or 8% w/v PEG 6000 by incubation at 4 °C overnight. Precipitated virus was harvested by centrifugation at 3,500*g* for 1 h at 4 °C and resuspended in 50 mM HEPES (4-(2-hydroxyethyl)-1-piperazineethanesulfonic acid), pH 7.5, containing 200 mM NaCl and 1% v/v NP-40, treated with 0.1% RNase A for 30 min on ice and again clarified by centrifugation at 3,500*g* for 1 h at 4 °C to remove insoluble particulates. Capsids were pelleted over a 3-ml, 30% sucrose cushion (in 50 mM HEPES, pH 7.5, containing 200 mM NaCl) at 105,000*g* for 2.5 h at 4 °C. Pellets were resuspended in HEPES buffer containing 0.5% (v/v) NP-40 overnight at 4 °C, clarified by centrifugation (16,000*g* for 10 min at 4 °C) and purified over a 15–45% sucrose gradient. The gradient was layered with the clarified supernatant containing virus and fractionated by centrifugation at 105,000*g* for 3 h at 4 °C. Fractions were analyzed by SDS-PAGE and subsequent Coomassie staining.

Purification of recombinant empty capsids. Mammalian cells dually infected with VV-FMDV and VV-T7 were harvested by centrifugation at 3,500*g* for 30 min at 4 °C, and pellets were resuspended in PBS. Frozen recombinant BV–infected Sf9 cell pellets containing overexpressed empty capsids were thawed and resuspended in 50 mM HEPES, pH 7.5, 200 mM NaCl and 1% NP-40. Cells were lysed by incubation with detergent for 30 min on ice. Lysates were clarified at 10,000*g* for 30 min at 4 °C, and capsids were pelleted over a 3-ml, 30% sucrose cushion by centrifugation at 105,000*g* for 5 h at 12 °C. Thereafter, recombinant capsids were purified as described for inactivated virus and analyzed by SDS-PAGE and subsequent Coomassie staining.

Negative-stain electron microscopy. Aliquots of purified samples were diluted to 0.2 mg/ml and deposited onto glow-discharged, Formvar/carbon-coated copper grids (Electron Microscopy Sciences). After a 30-s incubation, the excess sample was blotted away, and the grids were washed twice with deionized water. Samples were stained with 1% (w/v) uranyl acetate for 45 s, and excess stain was removed by blotting. Grids were examined on a Tecnai T12 transmission electron microscope operated at 80 kV. Images were acquired

on a 4,000 × 4,000 high-sensitivity FEI Eagle camera at 67000× magnification, which corresponded to 1.68 Å/pixel sampling of the specimen.

Thermostability and pH-stability assay for particles. Particle stability thermal release assay (PaSTRy)[29] was performed in 96-well PCR plates with an Agilent MX3005 PCR machine. All assays were performed with 300–500 ng of purified virus (3–15 µl) that had been dialyzed to remove most of the sucrose from purification. 15 µl of SYBR Green-II dye (Molecular Probes, Invitrogen) was diluted 1:100 in the same buffer as used for virus purification, and the volume was brought up to 150 µl with buffer. The temperature was ramped up from 25 °C to 95 °C in 0.5 °C increments at intervals of 10 s. SYBR Green-II fluorescence was read with excitation and emission wavelengths of 490 nm and 516 nm, respectively. The release of RNA, and hence the dissociation of capsids, was detected by an increase in fluorescence signal, and the melting temperature was taken as the minimum of the negative first derivative of the fluorescence curve.

ELISA. Wild-type or S93Y particles were incubated at 37 °C for up to 72 h, and their stability was analyzed by double-antibody sandwich ELISA with llama single-domain antibody fragments ((VHH domains), termed VHH M170, which binds intact FMD viral particles and VHH M3, which recognizes pentamer subunits). VHHs were provided by the Central Veterinary Institute of Wageningen UR)[30]. Microtiter-plate wells were coated with VHHs before the addition of serially diluted samples (in VHH buffer: 1% skimmed milk, 0.05% Tween, 0.5 M NaCl, 2.7 mM KCl, 2.8 mM KH_2PO_4, and 8.1 mM Na_2HPO_4, pH 7.4). After incubation for 1 h at 37 °C, biotinylated VHH M170 was then added and incubated for another 1 h at 37 °C. Plates were washed with PBS-Tween (0.05% Tween 20), and bound biotinylated VHH-M170F was visualized by incubation with streptavidin-HRP (Dako) for 1 h at 37 °C; this was followed by addition of *o*-phenylenediamine dihydrochloride (Sigma) for 15 min at room temperature. The reaction was stopped by addition of 1.25 M sulfuric acid and quantified at 492 nm with a Dynex microplate reader (Dynex Technologies).

Stability assay for recombinant empty capsids. Sucrose gradient–purified samples of FMDV empty capsids were diluted with PBS and incubated in a water bath at either 45 °C for 1 h or 56 °C for 2 h. They were then loaded onto 15–45% sucrose density gradients and sedimented. The gradients were fractionated from the bottom to the top, and an equal volume of saturated ammonium sulfate was added to 300 µl of each fraction to precipitate any empty capsids present. Pelleted precipitates were analyzed by SDS PAGE and western blotting for the VP1 capsid protein, with guinea-pig polyclonal antisera (**Supplementary Fig. 3**). In similar experiments, samples containing empty capsids were diluted with 50 mM sodium acetate buffer, pH 4.6, to produce a pH range of 5.5 to 6.5 (in 0.5 unit increments) and were incubated for 15 min at room temperature. After neutralization with 1/6 volume of 2 M NaOH[47], the empty capsids were loaded onto 15–45% sucrose density gradients and treated as described above before analysis by SDS PAGE and western blotting.

Crystallization, data collection and structure determination. Crystals were grown by the sitting-drop vapor-diffusion method in Crystalquick X plates (Greiner Bio-One) with 100 nl virus/empty capsids plus 100 nl precipitant dispensed with a Cartesian robot as described previously[48]. Microcrystals of inactivated O1M S93Y virus (2.2 mg/ml) and A22 H93F empty capsids (3 mg/ml) grew within 1 week at 294 K with either 1.5 M ammonium sulfate, 100 mM bis-Tris propane, pH 7.0, or 4 M ammonium acetate, 100 mM bis-Tris propane, pH 7.0, respectively. Optimization produced sufficient crystals for structural solution. A 20 × 20 µm^2 or 50 × 50 µm^2 beam (λ = 0.9778 Å; I24 microfocus beamline, Diamond), depending on the crystal size, was used for *in situ*[31] data collection at 294 K on a Pilatus 6 M detector.

The structures of O1M S93Y and A22 H93F were solved by molecular replacement with the coordinates and noncrystallographic symmetry (NCS) operators from O1BFS (PDB 1BBT)[22] and A22 (PDB 4GH4)[11]. Initial phase estimates were obtained by rigid-body refinement with CNS[49]. Twinned data sets were deconvoluted by combining five-fold NCS averaging in real space with rescaling individual reflections according to the twinning operator. This uses redundancy of information in the NCS to recover information lost by the superimposed 90°-rotation twinning operation. Iterative positional and *B*-factor refinement (via CNS) used strict NCS constraints. Phases were further improved by 15-fold (A22) and five-fold (O1M) NCS averaging. The percentages of Ramachandran outliers were 0 and 16.7 for A22 and O1M structures, respectively.

Cryo-EM data collection, structure determination and model building. Aliquots of 4 µl of purified inactivated O1M or SAT2 mutant S93Y virus were added on glow-discharged holey carbon-coated copper grids (C-flat, CF-2/1-2C; Protochips). Grids were blotted for 3 s, in 70% relative humidity, and vitrified in liquid ethane with a plunger device (Vitrobot; FEI). To increase the number of particles in the holes, grids were preincubated with 4 µl of sample for 30 s, and unbound sample was removed by blotting with filter paper.

Images were collected at 300 kV with a Tecnai F30 'Polara' microscope (FEI) equipped with an energy filter (GIF Quantum, Gatan) operating in zero-loss mode (0–20 eV energy selecting slit) and a direct electron detector (K2 Summit, Gatan). Movies (25 frames, each 0.2 s) were recorded at 1.0–3.0 µm underfocus in single-electron counting mode with SerialEM at a calibrated magnification of 37,027×, thus resulting in a pixel size of 1.35 Å. Frames from each movie were aligned and averaged to produce drift-corrected micrographs[50].

Structures were solved with RELION 1.3 according to recommended gold-standard refinement procedures[51], and icosahedral symmetry was applied. Micrographs showing signs of astigmatism or significant drift were discarded and not used for further analysis. Reference-free 2D class averaging was used to discard bad particles. The particle population was further improved by 3D classification. The X-ray structure of native FMDV A22 serotype (PDB 4GH4)[11] was low-pass-filtered to 50 Å and used as an initial template for 3D classification and refinement. A total of 8,267 O1M particles from 210 micrographs and 8,156 SAT2 particles from 321 micrographs were used to solve the final density maps at 3.2-Å and 3.5-Å resolution, respectively, as indicated by Fourier shell correlation and 0.143 cutoff (**Supplementary Fig. 7**). The O1M mutant was fitted in the density map as a rigid body with UCSF Chimera[52]. The fitting was further improved with real-space refinement with COOT[23]. The model of SAT2 was built with the SAT1 structure as a starting model with COOT[23]. REFMAC[53] was used to calculate the difference map, which highlighted the areas where the model was incorrect. Models were further improved by iterative positional and *B*-factor refinement in real space with Phenix[54] and COOT[23] iteratively. Only coordinates were refined; the maps were kept constant. Each round of model optimization was guided by cross-correlation between the map and the model. Statistics of refinement are given in **Supplementary Table 3**.

Vaccination of cattle and guinea pigs with stabilized FMDV vaccines. Four groups of four 100- to 150-kg male Holstein Friesian calves were vaccinated with either inactivated O1M-wt, O1M-(S93Y), SAT2-wt or SAT2-(S93Y) FMDV. Each animal received 15 µg of purified 146S antigen formulated in oil adjuvant ISA206B (SEPPIC) as an intramuscular injection on days 0 and 28 of the study. All 16 animals were bled to collect serum on days 0, 28, 35 and 42, and virus-neutralizing-antibody titers (VNT) were assessed. Animal experimentation was approved by the Pirbright Institute Ethical Review Board under the authority of a Home Office project license (70/7253) in accordance with the Home Office Guidance on the Operation of the Animals (Scientific Procedures) Act 1986 and associated guidelines.

For the guinea-pig experiments, inactivated SAT2 wild-type and stabilized mutant S93Y were formulated as commercial vaccines with oil-based ISA206B (SEPPIC) adjuvant and stored for 1 month at 4 °C. Aliquots containing 10 µg of 146S antigen at the time of formulation of these vaccines were then used to immunize two groups of ten adult inbred guinea pigs, aged 2-4 months. One group received the wild-type vaccine, whereas the other group received the stabilized vaccine. Serum samples were tested on day 0, and at 3 and 6 months pv, bleeds and virus VNT were assessed. The experiments were repeated with the same volumes after the vaccines had been stored for a total of 6 months at 4 °C. Serum samples were collected on days 0 and 30 pv, and the VNTs were analyzed. All studies in the Netherlands complied with the Dutch Experiments on Animals Act, February 5, 1997. All studies complied with the Council Directive 86/609/EEC on the approximation of laws, regulations and administrative provisions of the Member States regarding the protection of animals used for experimental and other scientific purposes.

No statistical method was used to predetermine sample size. Group sizes for the cattle and guinea-pig immunization studies were consistent with those in previously published studies used to determine the induction of antibody titers

consistent with protection[33,34]. No randomization was performed. The laboratory staff members performing the assessment of antibody titers were blind the animal group allocations.

Titration of neutralizing antibodies. Sera from guinea pigs and cattle were prepared from blood samples. Sera obtained at weekly intervals from day 0 to day 42 pv were assayed by a standard VNT test (OIE, 2012) on porcine kidney IB-RS2 cells with O1 Manisa and SAT2 wild-type viruses. Neutralizing-antibody titers, calculated by the Spearmann-Karber method, were expressed as the last dilution of serum that neutralizes 50% of the homologous virus (100TCID50)[44]. The mean antibody titers of each group of animals was compared with threshold antibody titers that have previously been shown to correlate with protection[33,34].

41. Bøtner, A. *et al*. Capsid proteins from field strains of foot-and-mouth disease virus confer a pathogenic phenotype in cattle on an attenuated, cell-culture-adapted virus. *J. Gen. Virol.* **92**, 1141–1151 (2011).
42. Zibert, A., Maass, G., Strebel, K., Falk, M.M. & Beck, E. Infectious foot-and-mouth disease virus derived from a cloned full-length cDNA. *J. Virol.* **64**, 2467–2473 (1990).
43. van Rensburg, H.G., Henry, T.M. & Mason, P.W. Studies of genetically defined chimeras of a European type A virus and a South African Territories type 2 virus reveal growth determinants for foot-and-mouth disease virus. *J. Gen. Virol*. **85**, 61–68 (2004).
44. Brehm, K.E., Ferris, N.P., Lenk, M., Riebe, R. & Haas, B. Highly sensitive fetal goat tongue cell line for detection and isolation of foot-and-mouth disease virus. *J. Clin. Microbiol.* **47**, 3156–3160 (2009).
45. Rieder, E., Bunch, T., Brown, F. & Mason, P.W. Genetically engineered foot-and-mouth disease viruses with poly(C) tracts of two nucleotides are virulent in mice. *J. Virol.* **67**, 5139–5145 (1993).
46. Berrow, N.S. *et al*. A versatile ligation-independent cloning method suitable for high-throughput expression screening applications. *Nucleic Acids Res.* **35**, e45 (2007).
47. Curry, S. *et al*. Viral RNA modulates the acid sensitivity of foot-and-mouth disease virus capsids. *J. Virol*. **69**, 430–438 (1995).
48. Walter, T.S. *et al*. A procedure for setting up high-throughput nanolitre crystallization experiments: crystallization workflow for initial screening, automated storage, imaging and optimization. *Acta Crystallogr. D Biol. Crystallogr.* **61**, 651–657 (2005).
49. Brünger, A.T. *et al*. Crystallography & NMR system: a new software suite for macromolecular structure determination. *Acta Crystallogr. D Biol. Crystallogr.* **54**, 905–921 (1998).
50. Li, X. *et al*. Electron counting and beam-induced motion correction enable near-atomic-resolution single-particle cryo-EM. *Nat. Methods* **10**, 584–590 (2013).
51. Scheres, S.H.W. RELION: implementation of a Bayesian approach to cryo-EM structure determination. *J. Struct. Biol*. **180**, 519–530 (2012).
52. Pettersen, E.F. *et al*. UCSF Chimera: a visualization system for exploratory research and analysis. *J. Comput. Chem.* **25**, 1605–1612 (2004).
53. Murshudov, G.N. *et al*. REFMAC5 for the refinement of macromolecular crystal structures. *Acta Crystallogr. D Biol. Crystallogr.* **67**, 355–367 (2011).
54. Wang, Z. *et al*. An atomic model of brome mosaic virus using direct electron detection and real-space optimization. *Nat. Commun.* **5**, 4808 (2014).

Supplementary Information

Supplementary Figure 1: Sequences and thermostability of cell culture–adapted particles at different pH values.

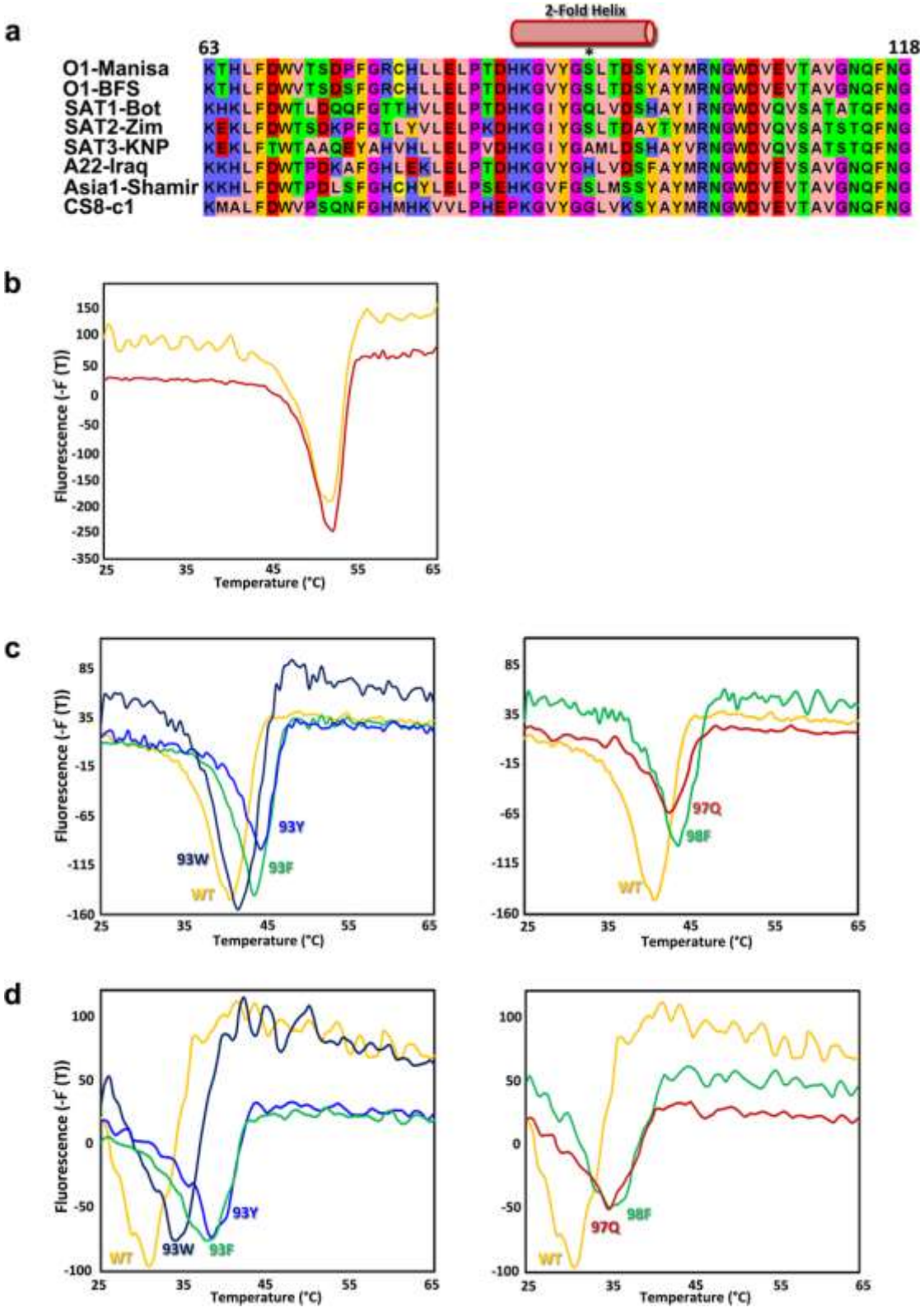

(**a**) Sequence alignment of a region of VP2 from representatives of seven FMDV serotypes (VP2 dominates the interactions at the inter-pentamer interface). The position of the α-helix found in all picornaviruses adjacent to the icosahedral 2-fold symmetry axis (residues 87-98) is shown as a red cylinder with position 93 indicated by a star (amino acid sequences are coloured using the Zappo Colour scheme in Jalview, **http://www.jalview.org/**). (**b**) The thermostability of infectious O1M wild type viruses with (HS+) and without (HS-) cell adaptation mutations remote from the pentamer interface were measured by fluorescence assay at pH 7.5. Both HS+ and HS- dissociated at 52.5˚C. (**c**) The engineered mutants are noticeably more thermostable at lower pH. At pH 7.0, the wild-type capsids dissociated at 41.0˚C (compared to 52.0˚C at pH 7.5, Figure 2b), S93Y dissociated at 43.5˚C, S93F at 42.5˚C, S93W at 41.5˚C, S97Q at 42.5˚C and Y98F at 43.4˚C. (**d**) At pH 6.5, the wild-type capsids dissociated at 30.5˚C, S93W dissociated at 34.0˚C and S93Y and S93F at 38.0˚C, whilst S97Q and Y98F dissociated at 34.0˚C.

Supplementary Figure 2: Effect of storage and heat treatment on inactivated wild-type and engineered O1M virus.

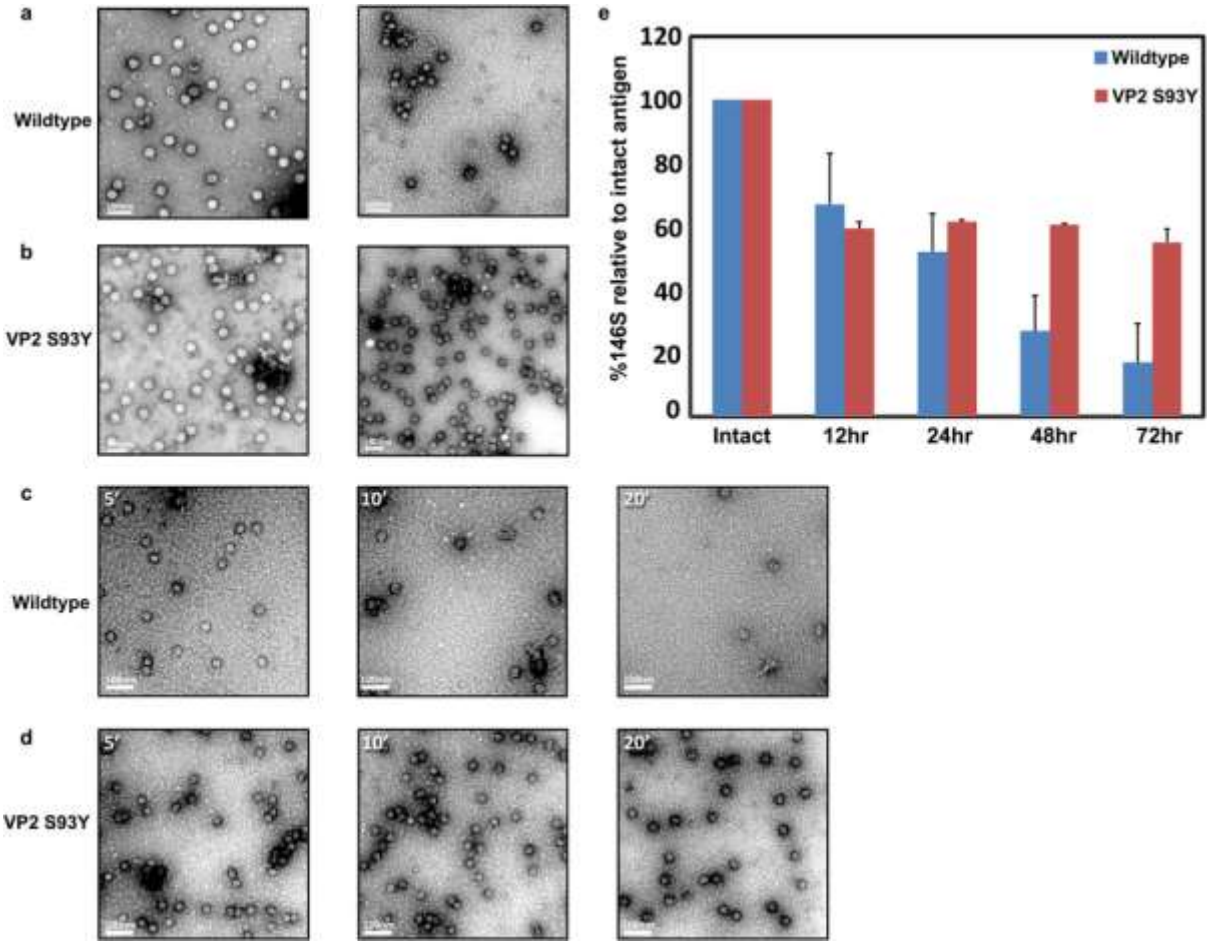

Purified inactivated O1M wild-type and S93Y mutant were analysed for intactness by negative stain EM. (**a**) ~10% of wild-type capsids are dissociated into pentamers when analysed soon after purification (quantified by taking the mean count of 5 independent areas on the grid), whereas S93Y particles appeared mostly intact. (**b**) Aliquots of the purified particles were stored at 4˚C and analysed again after ten days. ~80% of the wild-type capsids are dissociated into pentamers, whilst only ~10% dissociation is observed for the S93Y mutant (**c**) When incubated at 37˚C, wild-type O1M capsids readily dissociated into pentamers. After 20 min only ~5% capsids remained intact (taking the mean count of 5 independent areas on the grid compared to a similar mean count at time 0). (**d**) In contrast, S93Y mutant capsids were more resistant to heat treatment and ~60% capsids remained intact after 20 min. The scale bar indicates 100nm. (**e**) To further test the effect of storage, infectious O1M wild-type and mutant S93Y capsids were incubated at 37˚C for up to 72 h and aliquots analysed at 12, 24, 48 and 72 h post incubation by ELISA using single domain llama antibodies that specifically detect intact capsids (146S) or dissociated pentamers. Results are expressed as % of 146S particles relative to the intact antigen (starting antigen). After 72 h, ~50% mutant capsids remained intact whereas for wild-type ~15% capsids remained whole.

Supplementary Figure 3: Indirect sandwich ELISA for detection of FMDV O1Manisa.

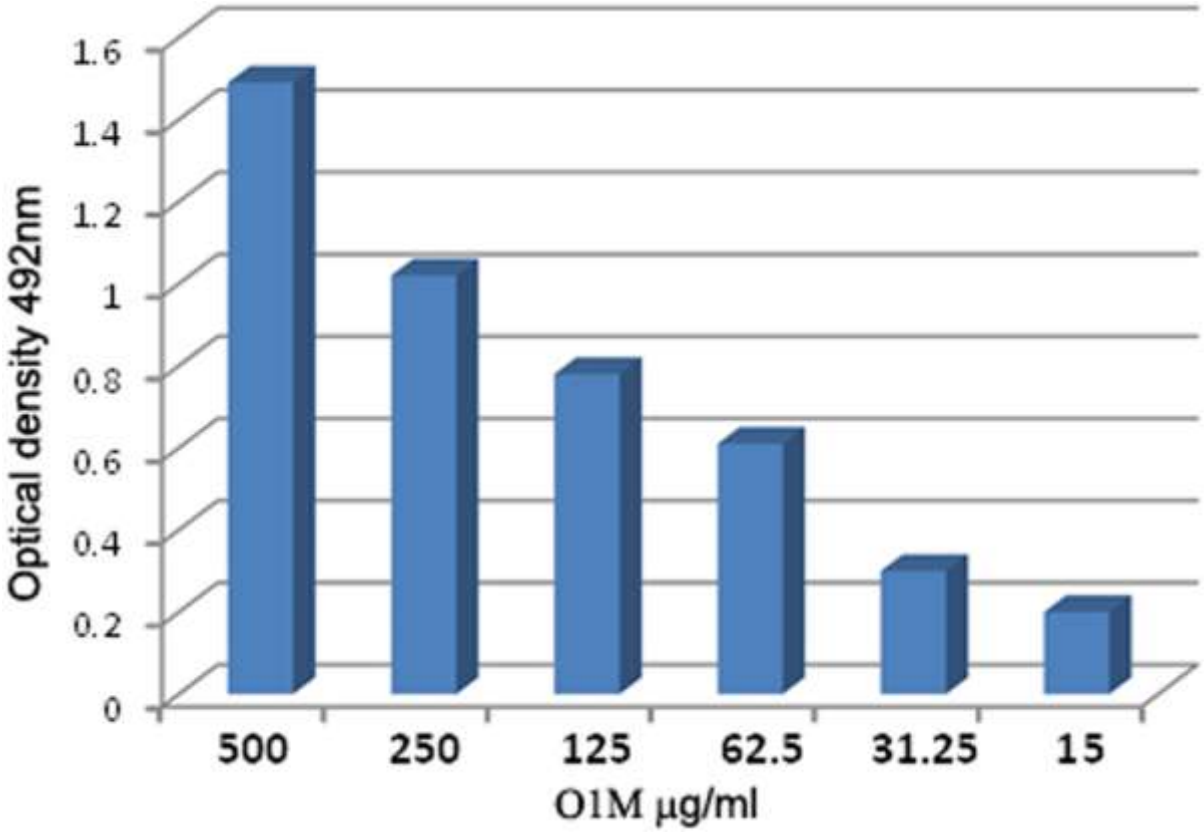

The guinea-pig polyclonal antisera to FMDV O1M used in this study was generated by immunization with inactivated, purified 146S (FMD) virus particles in Freund's Complete as shown previously (Ferris and Donaldson, 1984) and used in an indirect sandwich ELISA for FMDV antigen detection within the FAO World Reference Laboratory for Foot and Mouth Disease (WRL for FMD). Shown is an ELISA (Ferris et al., 2005) using a rabbit anti-FMDV type-O polyclonal serum as a trapping reagent for detection of a dilution series of inactivated, purified FMDV O1Manisa using the guinea-pig polyclonal antisera to O1Manisa as the primary antibody. Similar results were obtained for guinea-pig polyclonal antisera against FMDV A22.

Supplementary Figure 4: Thermostability of engineered O1M recombinant empty capsids.

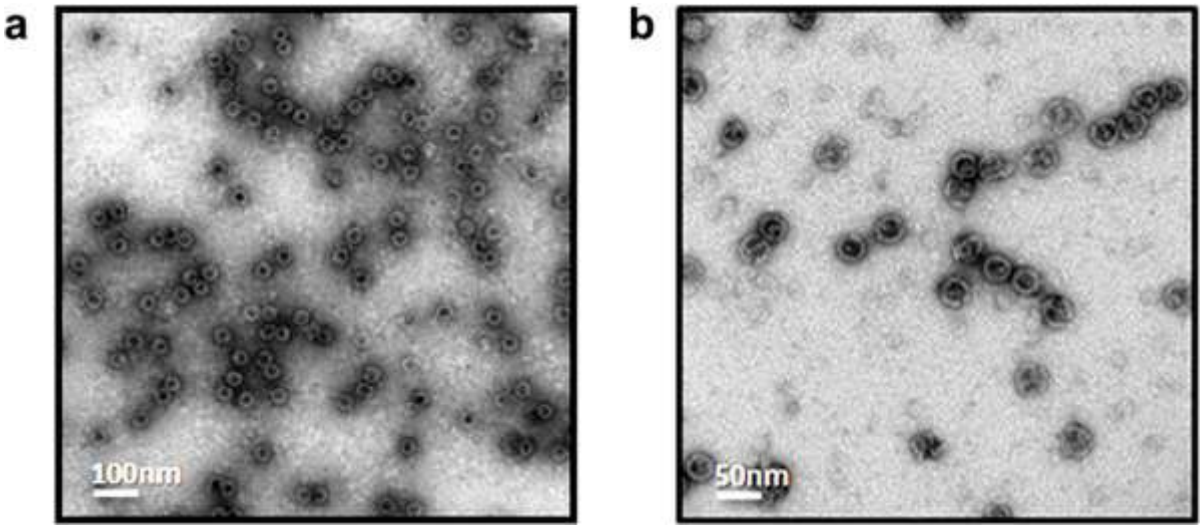

Recombinant S93F empty capsids were heated to 56˚C for 2 h and sedimented over a 15-45% sucrose gradient. The peak fraction was analysed by EM. (**a**) The empty capsids were found to be intact, further confirming their improved stability. The scale bar indicates 100nm. (**b**) High magnification image showing that ~90% capsids are intact. The scale bar indicates 50nm.

Supplementary Figure 5: Thermostability of engineered A22 recombinant empty capsids.

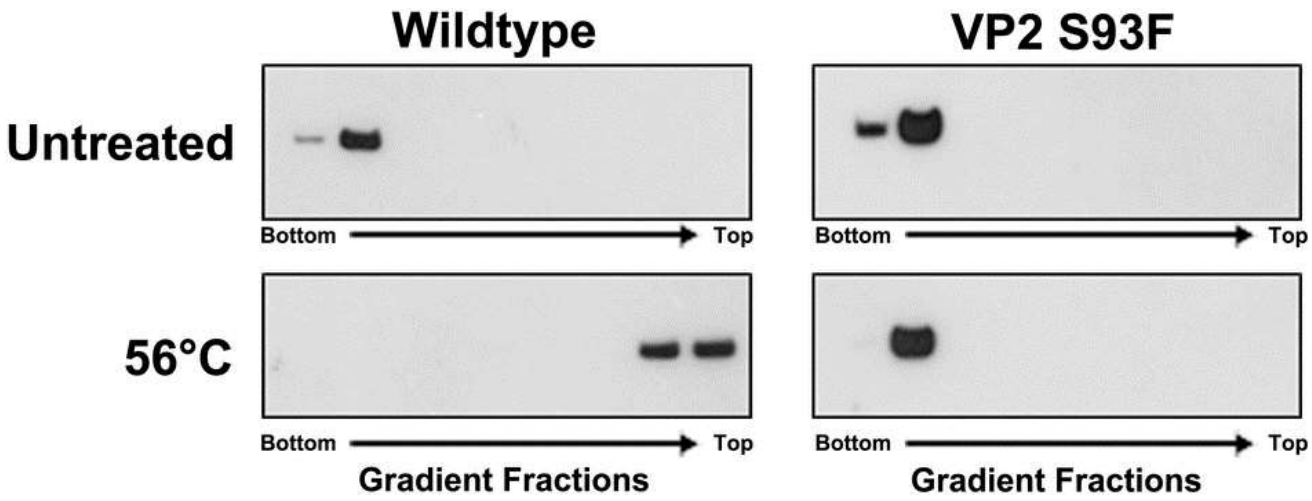

Purified capsids were left untreated or heated to 56˚C for 2 h and sedimented on 15-45% sucrose density gradients. Fractions were taken from the bottom of the gradients and analysed by western blot. Capsid proteins were detected using an anti-FMDV A22 polyclonal antibody. Heated H93F capsids remained intact and migrated to fractions 3-4, as did untreated capsids, whereas wild-type capsids dissociated upon heating, remaining near the top of the gradient.

Supplementary Figure 6: Stability of engineered O1M recombinant empty capsids upon storage at 37 °C.

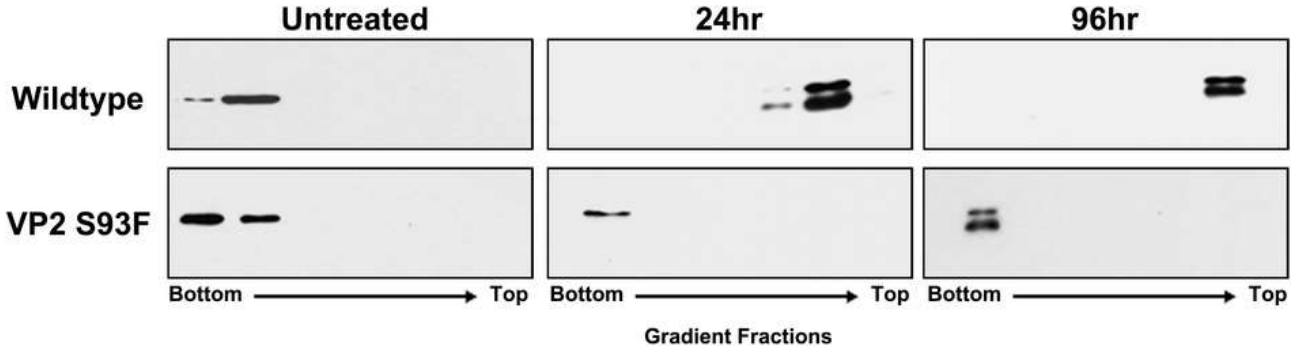

O1M wild-type and S93F empty capsids were incubated at 37˚C for 24 h or 96 h followed by sedimentation on 15-45% sucrose density gradients. Fractions were taken from the bottom of the gradients and analysed by western blot. Capsid proteins were detected using an anti-FMDV O1M polyclonal antibody. Wild-type capsids readily dissociated and remained near the top of the gradient, whereas mutant S93F capsids remained intact, even after 96 h.

Supplementary Figure 7: Cryo-EM analysis of stabilized FMDV particles.

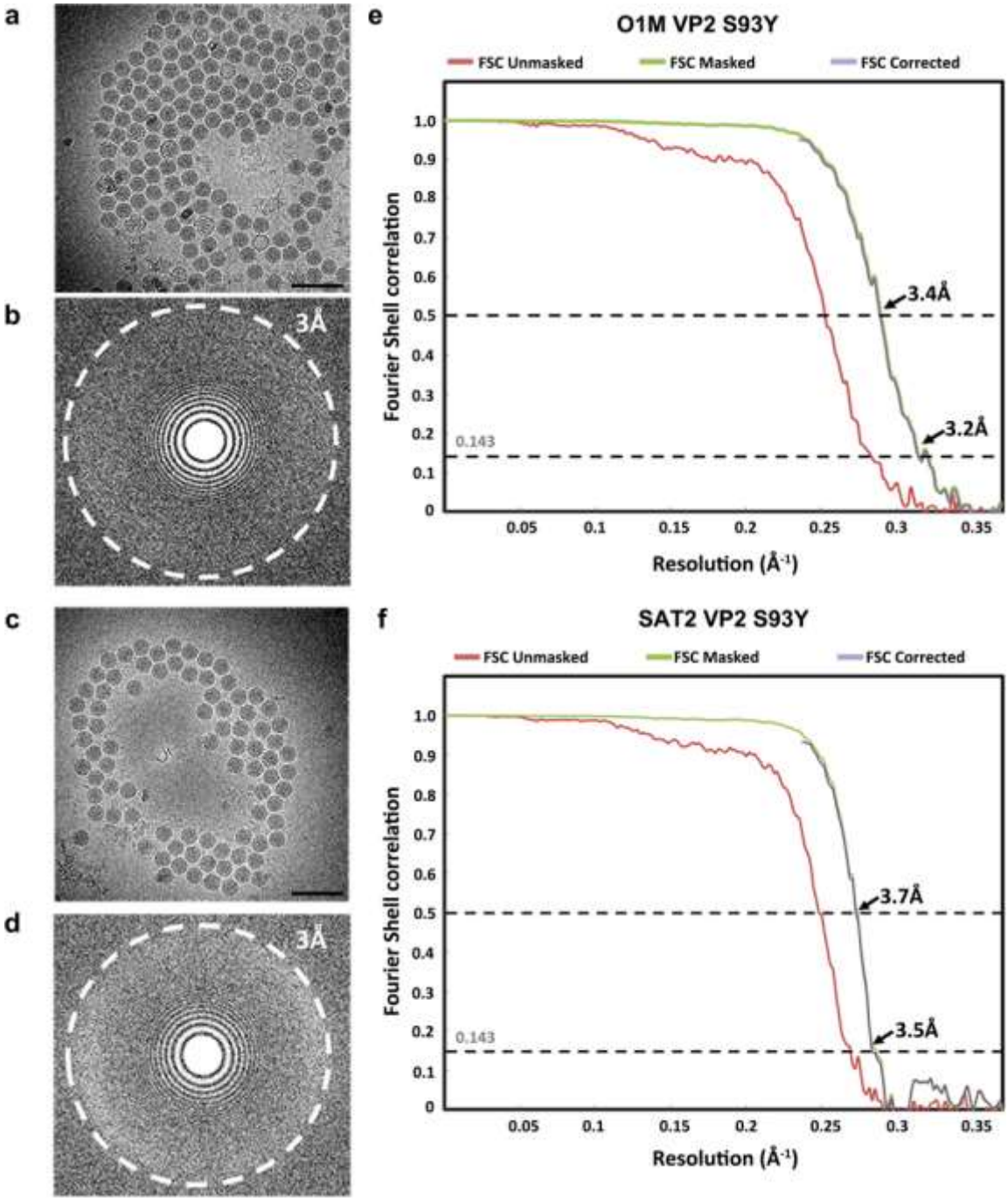

Purified inactivated O1M and SAT2 S93Y particles were used for data collection by cryoEM. (**a**) and (**b**) Representative aligned average (motion corrected) image of O1M VP2 S93Y particles and the corresponding Fourier transform. (**c**) and (**d**) Representative aligned average (motion corrected) image of SAT2 VP2 S93Y particles and the corresponding Fourier transform. (**e**) and (**f**) FSC curves of the final 3D reconstruction obtained using gold-standard refinement using RELION, marked with the resolution corresponding to a Fourier shell correlation (FSC) of 0.5 and 0.143. The scale bar indicates 100nm.